Short Communication

Hydrothermal Synthesis of Spindle-Like Nanostructured LiFePO$_4$ Powders Mediated by Organic Acid

Yatang Dai, Li Ma, Huan Zhang, Yuhua Chen, Yulei Chen, Wei Wang [*]

School of Materials Science and Engineering, Southwest University of Science and Technology, Mianyang 621010, China.
[*]E-mail: w.wang@swust.edu.cn

Well-crystallized spindle-like narrow size distribution (100~140 nm) LiFePO$_4$ nanoparticles for high rate lithium-ion battery cathode is synthesized via hydrothermal route employing amino tris(methylene phosphonic acid) (ATMP) as a surfactant. The samples are characterized by powder X-ray diffraction (XRD), dynamic Light Scattering (DLS), galvanostatic charge and discharge tests, scanning electron microscopy (SEM) and electrochemical impedance spectroscopy (EIS) measurements. Both the pure (F-blank) and with AMPT (F-AMPT) composites exhibit comparable capacities of 160.57 mAh g^{-1} and 132.53 mAh g^{-1} (0.1 C), 152.36 mAh g^{-1} and 121.36 mAh g^{-1} (0.5 C), and 126.57 mAh g^{-1} and 95.57 mAh g^{-1} (5 C), respectively. The capacity retention rates of F-AMPT sample over 50 cycles at 0.1 C is 95.57 % while F-blank yields 85.26 %. EIS measurements confirm that F-AMPT sample has an increased lithium ion diffusion coefficient of 1.62×10^{-12} cm^2 s^{-1} due to its higher surface area.

1. INTRODUCTION

Among a series of Li ion battery materials, olivine-type LiFePO$_4$ has been considered as one of the most important, dynamic, and promising materials for electric or hybrid carriers, due to its outstanding high-rate theoretical capacity, superior capacity retention, excellent thermal stability, highly reversible and repeatable property, nontoxicity, safety, environmental benignity and potentially low cost [1-3]. However, the extremely poor electronic conductivity and low lithium diffusion constant restrict its commercial application.

Recently, a lot of researchers have been devoted to ameliorate the intrinsic character of bulk LiFePO$_4$ or with extrinsic modifications to applicable level. Numerous effective approaches include reducing particle size [4], surface coating the active nanoparticles with ultra-thin carbon, generating homogeneous particle size distribution nanocomposites with compositing of polymers or doping metal

cationic ions, to enhance the electronic transport between the nanocomposites and $LiFePO_4$ [5, 6]. These efforts have been testified useful to short the diffusion length of electrons and lithium ions transport [7].

Zheng *et al.* [8] have prepared hollow $LiFePO_4$ nanoparticles by solvothermal method, which show excellent cycling capability. Tian *et al.* [9] synthesized $LiFePO_4/C$ nanorods with carbon coating by hydrothermal method. At high rates, the $LiFePO_4/C$ nanorods exhibit higher power densities, and better cycling performance. Cho *et al.* [10] have prepared core-shell $LiFe(PO_4)(OH)$ microspheres with the size distribution from 700 nm to more than 7 μ m. However, these methods are too complicated or require expensive reagents to prepare the uniform $LiFePO_4$ nanoparticles or nanocomposites.

In this paper, we report a simple one-pot synthesis method to prepare spindle-Like $LiFePO_4$ nanocrystals with narrow size distribution by a facile hydrothermal process mediated by inexpensive amino tris (methylene phosphonic acid) (ATMP) surfactant. The synthesized $LiFePO_4$ nanocrystals possess considerably high electronic conductivity, remarkable large surface area, and an improved lithium ion diffusion coefficient.

2. EXPERIMENTAL

2.1. Materials and preparation

In our experiment, $LiOH·H_2O$, $(NH_4)_2FeSO_4·7H_2O$ and H_3PO_4 were utilized as Li, Fe and P sources in the synthesis, respectively. In a typical experiment, 120 mmol $LiOH·H_2O$ and 40 mmol $(NH_4)_2FeSO_4$ were dissolved in 3 mL H_3PO_4 solution (14 mol L^{-1}) and 20 mL ascorbic acid solution (0.1mol L^{-1}), respectively. After that, the $LiOH/H_3PO_4$ solution was slowly dropwised into the mixture. Subsequently, 0.0024 mol ATMP was injected into the solution with stirring. Then the mixture was stirred at 25 ^{o}C for 5 min, and control the solution pH=8, by adding ammonia solution. For each time, 150 mL of the mixture was quickly transferred into the hydrothermal system (volume 250 mL). The hydrothermal reaction for preparing $LiFePO_4$ was carried out at 150 ^{o}C overnight. Finally, the $LiFePO_4$ precipitates were washed with Milli-Q water and ethanol at least 3 times. After dried in vacuum at 110 ^{o}C for 1 h, the precipitates were carefully collected. For the sake of comparison, phase-pure $LiFePO_4$ without ATMP was prepared in the parameters constant.

2.2. Characterization

The composition and phase of as-prepared spindle-Like $LiFePO_4$ nanoparticles were analyzed by X-ray diffraction (XRD) using Japan Neo-Confucianism Company. The morphologies of the samples were characterized by scanning electron microscope (SEM, Hitachi S-4800).

2.3. Electrochemical measurement

Electrochemical properties of $LiFePO_4$ samples were characterized by coin-type CR2025 lithium half-cells. The working cathode was prepared by 80 wt% $LiFePO_4$, 15 wt% acetylene black

and 5 wt% poly(vinylidenefluoride) (PVDF) binder in N-methyl-2-pyrrolidone to form a homogeneous slurry. Then, the slurry was coated on an Al foil current collector and dried at 120 ^{o}C for 10 h in a vacuum oven. After that, CR2025 coin-type cells were assembled in an argon-filled glove box by utilizing the metal lithium foils as the anode, the Celgard 2400 microporous membrane as the separator and 1M $LiPF_6$ solution in a mixture of ethylene carbonate (EC) and dimethyl carbonate (DMC) with a volumetric ratio of 1:1 as the electrolyte.

The galvanostatic charge and discharge tests were conducted in a potential range 2.5–4.2 V (*vs*. Li/Li$^+$) using a Land BT2001A automatic battery system at room temperature (RT, 25 °C). The electrochemical impedance spectroscopy (EIS) tests were performed by the IM6 electrochemical work station with the frequency ranging from 0.1 Hz to 100 kHz at a scanning rate of 5 mV s^{-1}.

3. RESULTS AND DISCUSSION
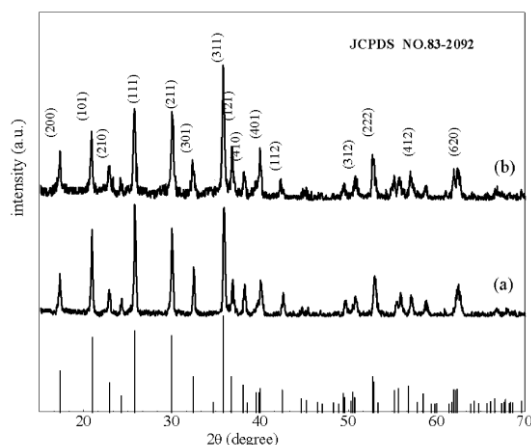
Figure 1. XRD patterns of as-prepared $LiFePO_4$ samples: (a) F-blank, (b) F-ATMP

Fig. 1 illustrates XRD results of as-synthesized $LiFePO_4$ nanoparticles with or without ATMP present. The $LiFePO_4$ nanoparticles show single phase, and the results are indexed well to the typical peaks of standard orthorhombic structure (JCPDS No. 83-2092). No impurities such as Li_3PO_4, trivalent Fe_2O_3 and $Li_3Fe_2(PO_4)_3$, which can be often found in the $LiFePO_4$ product prepared by traditional routes [11-13].

Fig. 2 shows SEM images of the as-synthesized spindle-Like $LiFePO_4$ nanoparticles. When ATMP is not applied, the obtained $LiFePO_4$ powders were aggregated with each other, which were 400 nm in wide and 200 nm in thickness. In contrast, the ATMP was proved to change the pattern of $LiFePO_4$ powders dramatically. As displays in Fig.2b, all of the individual crystals took the shape of discrete spindle-like particles with about 250 nm in length and 100 nm in diameter, indicating the useful of the appearance of the ATMP [14].
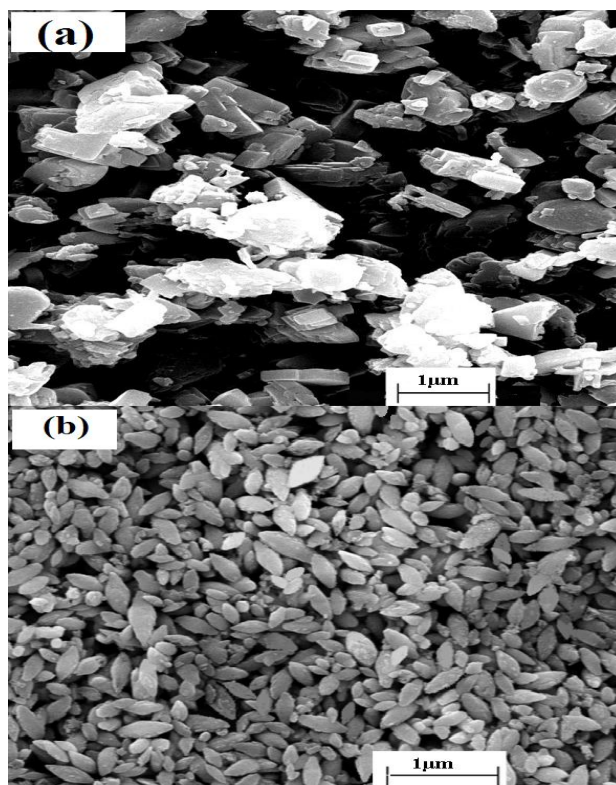
Figure 2. SEM images of the LiFePO$_4$ nanoparticles: (a) F-blank, (b) F-ATMP
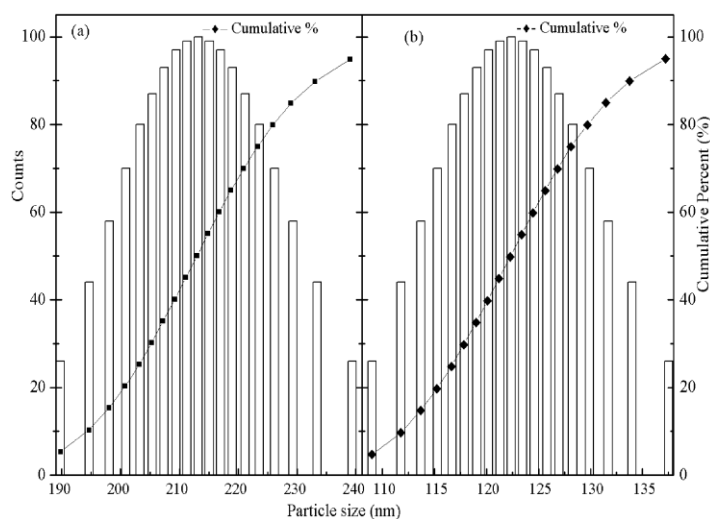
Figure 3. Size distribution of LiFePO$_4$ powders synthesized (a) without and (b) with ATMP

Fig. 3 shows the SEM images of the size distribution of LiFePO$_4$ nanoparticles. The images show that approximately 95% of F-AMPT is within 190–240 nm range with an average particle size (D_{50}) of ≈122 nm compared to that of ≈213 nm corresponding to the LiFePO$_4$ synthesized without the chelating agent. The result proves that the appearance of ATMP has effectively on the disperse of particles. The spindle-like LiFePO$_4$ nanoparticles show much smaller size and narrower size distribution.

3.2 Electrochemical measurements
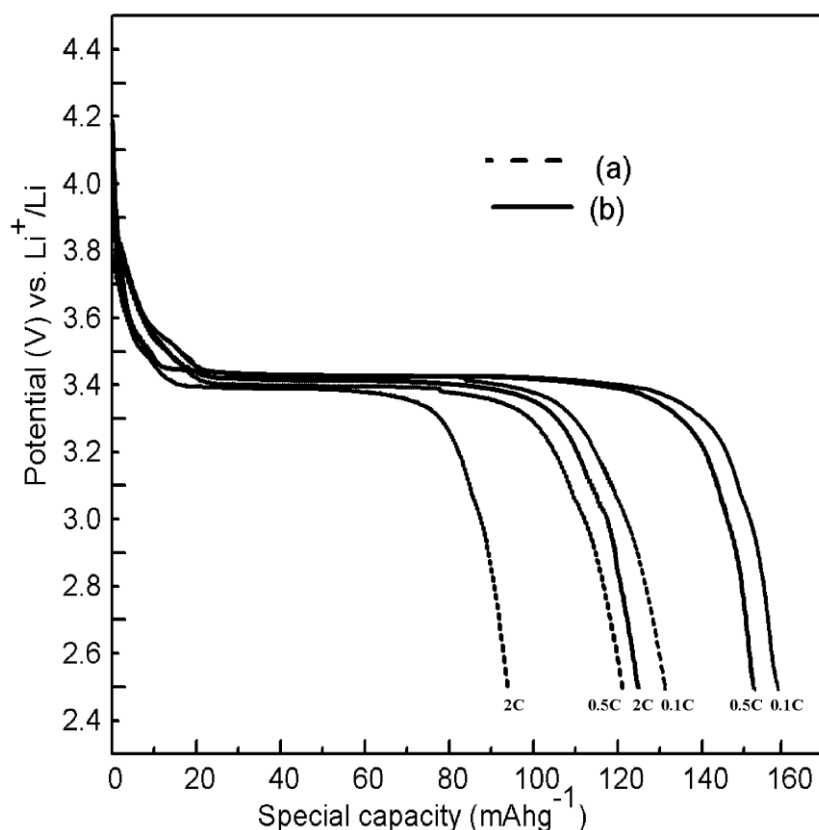
Figure 4. The initial discharge profiles of the LiFePO$_4$ synthesized (a) without ATMP and (b) with ATMP at various current rates (from 0.1 C to 2 C) between 2.5 V and 4.2 V at 25 °C.

Fig.4 shows the initial galvanostatic discharge curves of the LiFePO$_4$ cathodes at different current rates between 2.5 V and 4.2 V versus Li/Li$^+$ at room temperature. Both samples have similar discharge curves with flat plateaus corresponding to the lithium intercalation. The LiFePO$_4$ nanoparticles exhibit a flat plateau around 3.4 V for discharge voltage, corresponding well to the two-phase redox reaction between FePO$_4$ and LiFePO$_4$ system [15].

The spindle-like LiFePO$_4$ nanoparticles exhibit capacity of 160.57 mAh g^{-1} at 0.1 C, 152.36mAh g^{-1} at 0.5 C, and 126.57mAh g^{-1} at 2 C, whereas the LiFePO$_4$ synthesized without ATMP yields 132.53 mAh g^{-1} at 0.1 C, 121.36 mAh g^{-1} at 0.5 C and 95.57 mAh g^{-1} at 2 C, respectively. These results are comparable with the capacities values of other reports [12-16].

In addition, the spindle-like LiFePO4 nanoparticles electrode operated at 2 C exhibit 78.83% capacity retentions compared to its capacities at 0.1 C, which are higher than that of 72.11% for the LiFePO$_4$ synthesized without ATMP electrode. It is obviously that the spindle-like LiFePO$_4$ nanoparticles show much higher discharge capacity values and capacity retentions than the LiFePO$_4$ synthesized without ATMP.
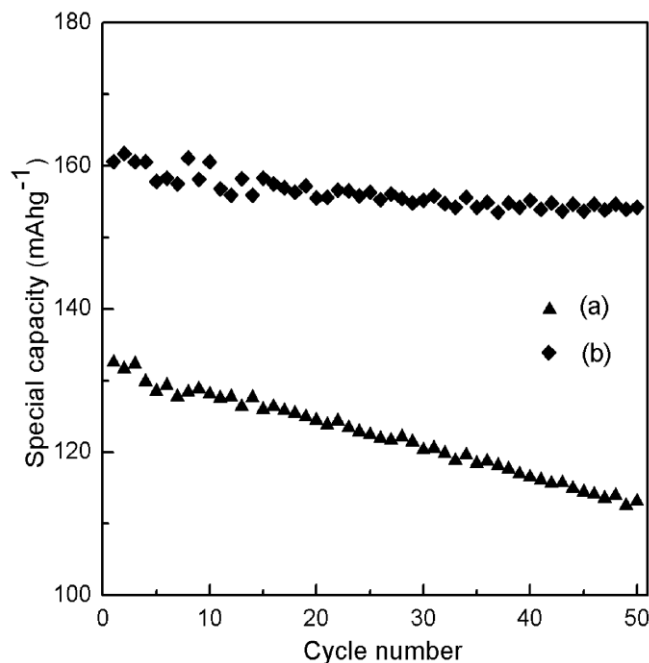
Figure 5. Cycle performances of LiFePO$_4$ (a) without and (b) with ATMP.
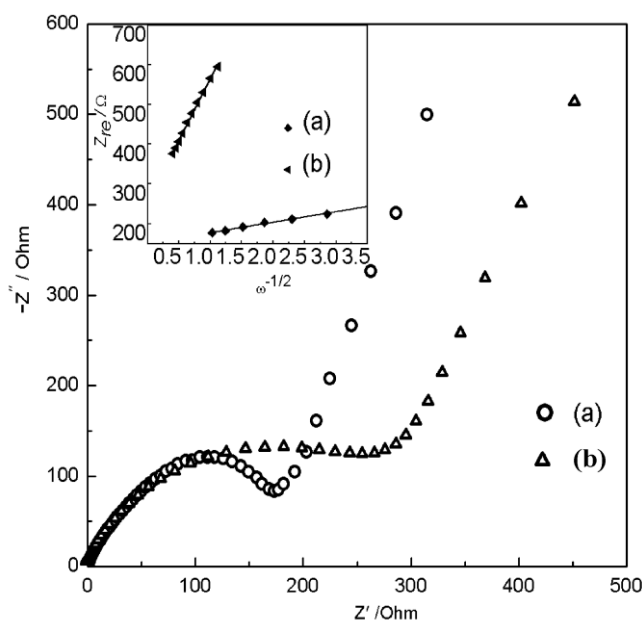
Figure 6. Electrochemical impedance spectroscopy (EIS) of LiFePO$_4$: (a) F-AMPT (b) F-blank and Inset graph of Z' plotted against $\omega^{-1/2}$.

Fig. 5 compares the cycling performance of as-prepared two samples over limited cycle at 0.1 C. Compared with the F-blank, the F-ATMP sample displays enhancement electrochemical performance. The F-ATMP discharges 153 mAh g^{-1} with capacity maintaining ratios of 95.57 %. In contrast, F-blank yields 113 mAh g^{-1} with capacity retention ratios of 85.26 %. It is obviously that the F-ATMP shows enhancing cycle performance of LiFePO$_4$, corresponding to its narrow and homogeneous particle size.

Subsequently, we characterized the electrochemical impedance spectroscopy in fully charged condition. Fig.6. presents Nyquist plots of LiFePO$_4$ electrodes with and without ATMP in the frequency range from 100 kHz to 10 mHz. As illustrated in Fig. 6, the impedance spectra can be explained according to an equivalent circuit with electrolyte resistance (R_e), charge transfer resistance (R_{ct}), double layer capacitance and passivation film capacitance (*CPE*) and Warburg Impedance (Z_w) [17]. Both profiles have a semicircle in the high-frequency region and a straight line in the low-frequency region, which are attributed to the charge-transfer resistance of electrochemical reaction and diffusion-controlled Warburg impedance, respectively [18]. The straight line is ascribed to the Warburg diffusion [15], and the lithium ion diffusion coefficient is calculated by the following equations [19, 20]:

$$D = R^2T^2 / 2A^2n^4F^4c^2\sigma^2 \quad (1)$$

$$Z_{re} = R_D + R_L + \sigma\omega^{-1/2} \quad (2)$$

where *A* is the electrode surface area, *n* is electrons per molecule during oxidization number, *F* is the Faraday constant, *R* is the gas constant, *T* is the absolute temperature, σ is the Warburg factor which can be obtained from the slope of the straight line of Z_{re}- $\omega^{-1/2}$ (Inset plot shown in Fig. 8), it corresponding to Eq. (2), *C* is the lithium ion concentration in LiFePO$_4$ electrode which is relative with.

$$c = n/V = m/MV = \rho V/MV = \rho/M \quad (3)$$

where ρ is the density, *M is* the molecular weight, *C* is calculated to be 5.67×10^{-3} mol cm^{-3} by Eq. (3). The lithium ion diffusion coefficient of F-ATMP sample is 1.62×10^{-12} cm^{2}s^{-1}, while the value of F-blank sample is 1.85×10^{-14}. It is apparently that the F-ATMP sample generates a higher lithium ion diffusion coefficient, due to the smaller spindle-like structure. The pathway for Li ion transfer of F-ATMP is short, which contribute to better electrochemical performance [21], corresponding to the charge and discharge results.

4. CONCLUSION

A spindle-like LiFePO$_4$ particle was synthesized by hydrothermal method in the presence of ATMP. SEM illustrates that the LiFePO$_4$ mediated by ATMP consists of nearly homogenous nanostructures with size of 100 nm; in contrast, the F-blank comprises large agglomerates.

Both the F-blank and F-AMPT composites exhibit comparable specific capacities of 160.57 mAh g^{-1} vs. 132.53 mAh g^{-1} at 0.1 C, 152.36 mAh g^{-1} vs. 121.36 mAh g^{-1} at 0.5 C, and 126.57 mAh g^{-1} vs. 95.57 mAh g^{-1} at 5 C, respectively. The capacity retention rates of F-AMPT samples over 50 cycles at 0.1 C is 95.57% (vs. the first-cycle corresponding C-rate capacity) while F-blank yields 85.26%. The spindle-like LiFePO$_4$ nanoparticles with small size and narrow size distribution produced excellent electrochemical performance, due to their rough surfaces. It is believed that the spindle-like morphology increases the contact area between the spindle-like LiFePO$_4$ nanoparticles and the electrolyte and reduces the Li$^+$ diffusion length.

References

1. N. Yabuuchi, K. Yamamoto, K. Yoshii, I. Nakai, T. Nishizawa, A. Omaru, T. Toyooka and S. Komaba, *J. Electrochem. Soc.*, 160 (2013) A39-A45.
2. B. Jin and H. B. Gu, *Solid State Ionics*, 178 (2008), 1907-1914.
3. Z. G. Lu, H. L. Chen, R. Robert, B. Y. X. Zhu, J. Q. Deng, L. J. Wu, C. Y. Chung and C. P. Grey, *Chem. Mater.*, 23 (2011) 2848-2859.
4. K. Dokko, S. Koizumi, K. Sharaishi and K. Kanamura, *J. Power Sources*, 165 (2007) 656-659.
5. J. Z. Li, S. Y. Wang, L. H. Wei, Z. Liu and Y. W. Tian, *Int. J. Electrochem. Sc.*, 10 (2015) 6135-6145.
6. B. Pei, Q. Wang, W. X. Zhang, Z. H. Yang and M. Chen, *Electrochim. Acta*, 56 (2011) 5667-5672.
7. X. Y. Zhang, M. van Hulzen, D. P. Singh, A. Brownrigg, J. P. Wright, N. H. van Dijk and M. Wagemaker, *Nat. Commun.,* 6 (2015).
8. Z. M. Zheng, W. K. Pang, X. C. Tang, D. Z. Jia, Y. D. Huang and Z. P. Guo, *J. Alloy. Compd.*, 640 (2015) 95-100.
9. R. Y. Tian, G. Y. Liu, H. Q. Liu, L. N. Zhang, X. H. Gu, Y. J. Guo, H. F. Wang, L. F. Sun and W. G. Chu, *RSC Adv.,* 5 (2015) 1859-1866.
10. M. Y. Cho, Y. S. Lim, S. M. Park, K. B. Kim and K. C. Roh, *Crystengcomm.,* 17 (2015) 6149-6154.
11. L. Wang, W. T. Sun, X. Y. Tang, X. K. Huang, X. M. He, J. J. Li, Q. W. Zhang, J. Gao, G. Y. Tian and S. S. Fan, *J. Power Sources*, 244 (2013), 94-100.
12. R. Shahid and S. Murugavel, *Phys. Chem. Chem. Phys.,* 15 (2013) 18809-18814.
13. Y. Xia, W. K. Zhang, H. Huang, Y. P. Gan, J. Tian and X. Y. Tao, *J. Power Sources*, 196 (2011) 5651-5658.
14. G. Meligrana, C. Gerbaldi, A. Tuel, S. Bodoardo and N. Penazzi, *J. Power Sources,* 160 (2006) 516-522.
15. J. L. Liu, R. R. Jiang, X. Y. Wang, T. Huang and A. S. Yu, *J. Power Sources*, 194 (2009) 536-540.
16. D. Choi and P. N. Kumta, *J. Power Sources*, 163 (2007) 1064-1069.
17. G. H. Qin, S. Xue, Q. Q. Ma and C. Y. Wang, *Crystengcomm*, 16 (2014) 260-269.
18. L. Wang, L. B. Yang, L. Gong, X. Q. Jiang, K. Yuan and Z. B. Hu, *Electrochim. Acta,* 56 (2011) 6906-6911.
19. Y. D. Liu, Q. Liu, Z. F. Li, Y. Ren, J. Xie, H. He and F. Xu, *J. Electrochem. Soc.,* 161 (2014) A620-A632.
20. O. A. Drozhzhin, M. A. Vorotyntsev, S. R. Maduar, N. R. Khasanova, A. M. Abakumov and E. V. Antipov, *Electrochim. Acta,* 89 (2013) 262-269.
21. X. Y. Wang, H. Hao, J. L. Liu, T. Huang and A. S. Yu, *Electrochim. Acta,* 56 (2011) 4065-4069.